Princeton Plasma Physics Laboratory

PPPL-5125

Simulations of non-inductive current rampup and sustainment in the National Spherical Torus Experiment Upgrade

F. M. Poli, R.G. Andre, N. Bertelli, S.P. Gerhardt, D. Mueller, G. Taylor

July 2015

PPPL PRINCETON PLASMA PHYSICS LABORATORY

Prepared for the U.S. Department of Energy under Contract DE-AC02-09CH11466.

Princeton Plasma Physics Laboratory
Report Disclaimers

Full Legal Disclaimer

Trademark Disclaimer

PPPL Report Availability

Princeton Plasma Physics Laboratory:

http://www.pppl.gov/techreports.cfm

Office of Scientific and Technical Information (OSTI):

http://www.osti.gov/scitech/

Related Links:

U.S. Department of Energy

U.S. Department of Energy Office of Science

U.S. Department of Energy Office of Fusion Energy Sciences

Simulations of non-inductive current rampup and sustainment in the National Spherical Torus Experiment Upgrade

F. M. Poli, R.G. Andre, N. Bertelli, S.P. Gerhardt, D. Mueller, G. Taylor

Princeton Plasma Physics Laboratory, Princeton, NJ, 08543, USA.

E-mail: fpoli@pppl.gov

Abstract. The start-up, ramp-up, and sustainment of a tokamak plasma utilizing little to no induction from a central solenoid is a major challenge in magnetic fusion. Future Fusion Nuclear Science Facilities based on the Spherical Tokamak design are projected to rely on Neutral Beam Injection to sustain about half of the plasma current in steady-state, with the remainder provided by the self-generated bootstrap current, and to provide heating and current drive for non-inductive current ramp-up. This work discusses predictive simulations of non-inductive ramp-up and sustainment on the National Spherical Torus Experiment Upgrade. Radio-Frequency waves at harmonics higher than the ion cyclotron resonance (HHFW) and Neutral Beam Injection are combined to ramp the plasma current non-inductively. Simulations indicate that density feedback control and current profile control will be necessary in order to attain the desired target. It is shown that the addition of Electron Cyclotron wave heating can significantly increase the effectiveness of the radio-frequency power and relax the requirements on the total level of power that needs to be coupled to the startup plasma.

PACS numbers:

1. Introduction

The Spherical Torus (ST) [1, 2] is a leading candidate for a Fusion Nuclear Science Facility (FNSF) due to its compact size and modular configuration [3, 4]. The high neutron wall load, the high values of β (plasma pressure to magnetic pressure ratio) achievable and the ease of maintenance make the ST an attractive option for nuclear component test facilities [5].

Critical elements of ST research in support of steady-state operation and demonstration of the viability of the ST as a fusion power plant include sustainment of fully non-inductive current with large bootstrap fraction [5, 6], non solenoidal startup and ramp-up [5] and operation at high β and high confinement with Resistive Wall Mode stabilization [7].

The start-up, ramp-up, and sustainment of a tokamak plasma utilizing little to no induction from a central solenoid is a major challenge in magnetic fusion. In particular, the development of techniques to minimize or eliminate the central solenoid is critical to the design of compact electricity-producing fusion power plants based on the ST concept and could also benefit advanced tokamak reactors. Eliminating the central solenoid would simplify engineering design and reduce costs.

The method of coaxial helicity injection (CHI) relies on electrostatic helicity injection for initiating the plasma discharge [8]. Transient CHI has successfully demonstrated the formation of high-quality closed flux plasma in NSTX with a flux saving with respect to ohmic startup [9, 10, 11] and will be used as a front end of the start-up method for a full demonstration of non-inductive current startup [12]. Simulations project CHI to be capable of generating over 400-600 kA of closed flux surfaces in NSTX-U, operating at full field [5, 12].

Future ST-FNSF are projected to rely on Neutral Beam Injection (NBI) to sustain about 50% of the plasma current, with the remainder provided by the self-generated bootstrap current. In addition, NBI is also envisioned to provide heating and current drive for non-inductive current ramp-up. In order to assess non-inductive advanced scenarios for ST-FNSF, the National Spherical Torus eXperiment (NSTX-U) is undergoing a major upgrade to double the toroidal field from 0.55 T and 1 s duration to 1 T and 6 s duration. The additional flux available in the new ohmic coil will allow the sustainment of up to 2 MA of current for 5 s at full magnetic field [5].

Extensive simulations have been previously undertaken to define the equilibrium operating space in NSTX-U [6]. Scenarios were defined over fully relaxed equilibria, extrapolating from experimental NSTX density and temperature profiles. Thermal pressure peaking, Greenwald density fraction, thermal ion transport and outer gap were identified as critical elements in determining the operational space. This work discusses time-dependent simulations of current ramp-up and sustainment with NBI and Radio Frequency (RF) waves, and discusses some of the issues that require validation and that need to be addressed in experiments. The simulations, run with free-boundary TRANSP [13, 14], evolve self-consistently the equilibrium, the heating and current drive sources

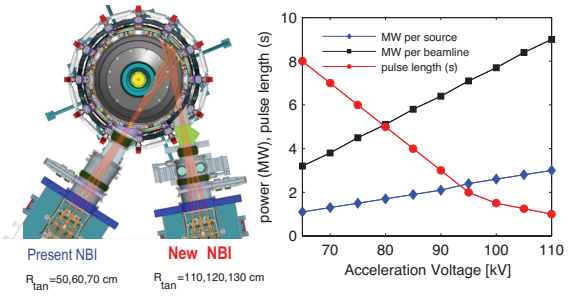

Figure 1. Left: layout of the beamlines. The present NBI has three sources at tangency radius of 50, 60, 70 cm; the second NBI has also three sources, more tangential, at 110, 120, 130 cm. Right: power per source (diamonds), power per beamline (squares) and pulse length (circles) for each value of source voltage.

and the pressure profiles, within the limits of the physics model used to predict energy transport. Self-consistent evolution is particularly important in the non-inductive ramp-up. Pressure and externally driven current profiles undergo variations over short time scales and may exhibit large spatial gradients. The equilibrium and the kinetic profiles must be evolved self-consistently, while ensuring at the same time adequate control of the plasma position and shape.

Description of the Heating and Current Drive sources and of the modeling tools is given in Sec.2. Section 4 discusses a simulation scenario where the two beamlines are used in combination with RF waves to ramp-up the current non-inductively to 0.8 MA. Section 5 discusses issues with using individual sources at startup. Section 6 shows how using EC waves for heating the startup plasma would improve the absorption of RF waves and close the gap between the CHI startup and the current ramp-up with HHFW and NBI. Finally, conclusions and future plans for experiments and validation are addressed in Sec.7.

2. Heating and Current Drive systems and calculations.

Neutral Beam Injection. A second Neutral Beam system will add three sources to the existing, small tangency radius beamline, doubling the external heating and current drive capabilities. The second beamline, with tangency radii of 110, 120, 130 cm respectively, is designed to provide 100% non-inductive current for discharges with up to 1.3 MA [5].

Figure 1 shows the NB layout and summarizes the power and beam pulse duration as a function of the source voltage. Due to thermal limits of the ion dumps, the available pulse length on each beamline is reduced from 5 s to about 1.0 s as the beam energy and the total power available are increased from 3.3 MW (three sources with 65 kV) to 9 MW (three sources with 110 kV) [5]. Compared to the small tangency radius beamline, the larger tangency radius is projected to increase the current drive efficiency by 40%, opening opportunities for control of current profiles and q_{min}, for accessibility to high

performance plasmas [6]. The NB source model is the NUBEAM orbit following Monte Carlo code [15, 16], with current drive calculations that include collisionality dependence on shielding factor at arbitrary aspect ratio [17].

High Harmonic Fast Waves. Fast waves at high harmonics of the ion cyclotron frequency are launched on NSTX-U at a frequency of 30 MHz with a large 12 strap antenna array that spans 90 degrees toroidally around the outside of the torus [18]. Spectra corresponding to parallel wavevectors of 3, 8, 13 m^{-1} can be selected by feeding the antenna with six decoupled sources [19]. The doubling of the magnetic field, while retaining the 30 MHz RF source frequency, moves the heating regime from the high harmonic used in NSTX to a mid harmonic fast wave regime. In particular, for deuterium majority ion and 0.55 T in NSTX the harmonic resonances inside the last close flux surface range from the 2nd/3rd to the 11th whereas, for 1 T, the harmonic resonances inside the last close flux surface range from the 2nd to the 5th [20].
The HHFW system is used in the simulation scenarios discussed herein to heat the startup plasma, to assist with the L-H transition and to sustain up to 400 kA of non-inductive current during the time window where the NB cannot effectively drive current, because of large shine-thru at low density.
The ICRF source model is the TORIC full wave [21] with an equivalent Maxwellian treatment for the fast ion species. The effective temperature of beam ions is calculated as $2E/3n_{fast}$, where the fast ion density n_{fast} is calculated by NUBEAM and E is the averaged energy of the fast ion distribution, assuming a Maxwellian distribution.

Electron Cyclotron waves heating. Electron Cyclotron Waves heat the plasma at the electron cyclotron resonance, which is given by f[GHz]=$28B_T$[T]. At this frequency, the waves are injected with O-mode polarization (with the wave electric field parallel to the magnetic field). With this polarization, the EC waves have a cut-off frequency at the electron plasma frequency $\omega_{pe} = (4\pi\ n_e e^2/m_e)^{0.5}$, where e and m_e are the electron charge and mass and n_e the electron density.
A megawatt-level 28GHz electron cyclotron heating system is currently planned as an upgrade in NSTX-U in 2017-18 [22, 23]. The gyrotron can deliver up to 1 MW of power to the plasma over a pulse length of 1-5 s. The power will be transmitted via a low-loss, 50 mm diameter, corrugated $HE_{1,1}$ waveguide [22, 23].
On NSTX-U and for 1 T magnetic field and a frequency of 28 GHz, the EC waves have a cutoff for the O-mode at a density of 9.72×10^{18} m^{-3}. This limits the application of EC heating in NSTX-U to the early ramp-up phase.
The orientation of the mirror is fixed, pointing 5 degrees down and 1 degree right of the normal of the ECRH port. This is the position that maximizes first pass absorption, as it has been demonstrated by previous ray-tracing calculations over a typical CHI plasma target [22]. This steering injection configuration maximizes the electron heating, with minimum current drive.
The electron cyclotron heating and current drive are calculated with the GENRAY

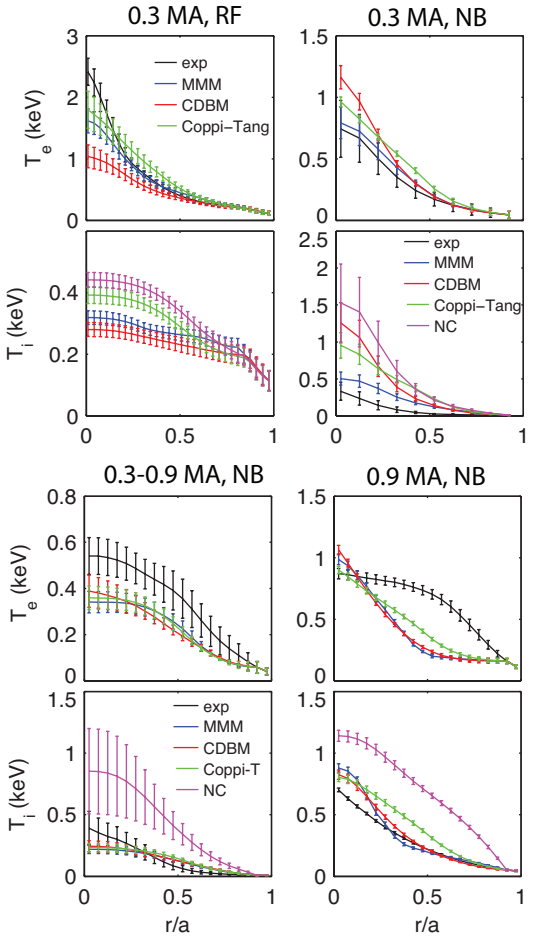

Figure 2. Comparison between the measured electron temperature and the temperature predicted under different assumptions of the thermal transport, for NSTX discharges with RF and with NBI. Top panel: 300kA flattop plasma with RF (left) and with NB (right). Bottom panel: 900kA discharge with 5MW of NBI, average profiles in the rampup (left) and in the flattop (right).

toroidal ray tracing code [24, 25], which includes an adjoint calculation of the electron cyclotron current drive efficiency that takes into account relativistic effects, trapped particle effects and momentum conserving corrections to the background collision operator [26, 27].

3. Transport assumptions

Predictive simulations rely on the thermal transport model used. Assessment of transport in H-mode will be undertaken in NSTX-U, including pedestal structure, L-H transition threshold, characterization of NB deposition, heating and current drive. In the absence of validation against NSTX-U like conditions, the simulations discussed herein are based on the results from transport models applied in NSTX plasma conditions.
A number of NSTX discharges that are representative of the plasmas simulated herein

have been selected, where HHFW will be used to ramp the current after startup to values of 300-400 kA and where NBI will be used afterwards for ramp-up to full current and sustainment. However, it should be noted that these reference cases, where the external sources are used in the flattop phase, do not describe the transient conditions of the plasma after startup. Experiments on NSTX-U with beam overdrive and HHFW injection on low density, low temperature startup plasmas, will be deemed necessary for a validation of the transport in this phase and for self-consistent projections from NSTX-U experiments to fully non-inductive startup and current ramp-up in FNSF.
The cases selected include (a) a plasma with 300 kA current and 1.5 MW of HHFW that achieves fully non-inductive current drive operating at low density to maximize the current drive efficiency (#138506) [28], (b) a 300 kA discharge with 1.5 MW of NBI (#140353), run for comparison with the RF discharge and (c) a 900 kA discharge with 200 ms ramp-up and NBI from the ramp-up phase (#142305) [29]. The latter will be also used as a reference for projections of non-inductive current ramp-up and sustainment in NSTX-U.
Figure 2 shows a comparison between the measured temperature and the temperature predicted under different assumptions on the thermal transport. Simulations have been run first with TRANSP in interpretive mode, then in predictive mode using various transport models: the MultiMode MMM7.1 [30], Coppi-Tang [31], the Current Diffusive Ballooning Mode model (CDBM) with plasma shape corrections [32] for both the ion and electron channel and neoclassical transport for the ion thermal transport, using the NCLASS NTCC libraries [33]. The profiles shown in Fig.2 have been averaged over the heating phase for both the flattop cases and the ramp-up heated phase with NBI. The error bars indicate the standard deviation from the average value during the heated phase.
In flattop discharges with 300 kA (top panel in Fig.2), no model is systematically over- or under-predicting the electron or the ion temperature, with the CDBM giving the lowest average temperature in the RF heated discharge and the highest average value in the NBI heated discharge. The MMM7.1 model can reproduce the peaked profiles better than other models and in the NBI heated discharge at low current gives the closest agreement with the experiments. Ion temperature measurements are not available in RF-only discharges and no conclusion can be drawn here on what model reproduces the experiments better. It should be noted that these plasmas are in L-mode.
In the discharge with NBI at 900 kA (bottom panel in Fig.2), all models agree with each other, but none of them can reproduce the broad electron temperature profile in the flattop. A good agreement among the turbulence models is also found in the ion temperature predictions, all in better agreement with experiments than the Neoclassical model, which tends to over-predict the ion temperature in all cases. In the ramp-up phase of the large current, NBI heated discharge, a good agreement is found among models and between models and experiment.
Based on this comparison, we have selected the MMM7.1 model for prediction of thermal transport in the electron and ion channel in the early ramp-up phase, up to 400 kA,

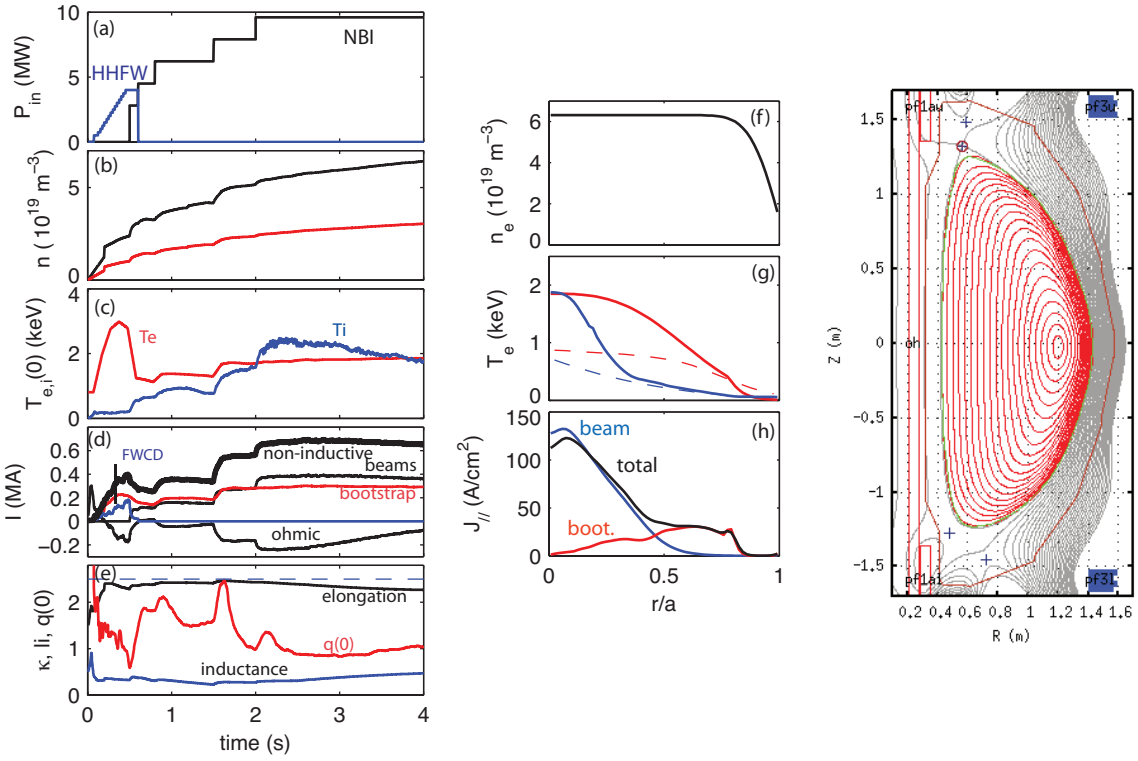

Figure 3. Left panel: (a) injected power, (b) central and line averaged electron density, (c) central electron and ion temperature, (d) contributions to the current, (e) safety factor on-axis, elongation at the separatrix and internal inductance for a simulation discharge with density of $0.75n_{\rm G}$. Central panel: profiles of (f) density, (g) electron and ion temperature from the simulation and from the reference discharge (dashed) , (h) current density at 3.5 s. Right panel: equilibrium calculated at 3.5 s.

where RF will be primarily used, either alone or in combination with NBI. During the NBI phase, where the current is ramped-up to 900 kA over a time window that spans between 2.5 and 5 s, analytic temperature profiles are used for the electron channel and the MMM7.1 is used for the ion channel.

It should be noted that the predictive simulations in the NBI heated, flattop plasma, are not making any assumptions on the fast ion diffusion coefficients, which causes all the models to predict profiles that are far too peaked compared to experiments. An appropriate analysis would require changing the coefficients until the plasma parameters are matched, including the neutron rate. Then, hypotheses on the fast-ion diffusion in NSTX-U would have to be made, and uncertainties taken into account. It has been decided to reduce the number of assumptions on transport issues that need validation and to use analytic profiles for the electron temperature.

4. Current ramp-up and sustainment

Plasma discharge #142305 discussed above is chosen as a reference for time-dependent simulations to project to non-inductive ramp-up and sustainment in NSTX-U. This discharge was part of an experimental campaign targeting high-performance, higher elongation and aspect ratio plasmas, developed specifically in support of NSTX-U and of next-step ST devices in general. Those experiments were extensively discussed by Gerhardt *et al* [29] and the specific case chosen as a basis for our studies is plotted in Fig. 22 of that article.

The reference discharge provides most of the input parameters for the predictive simulation: density profile, reference ion and electron temperature, profile for the dominant impurity (Carbon), rotation profile and effective ion charge Z_{eff}. Time-dependent simulations have been run with TRANSP with the free boundary `Isolver` [14], to evolve the plasma discharge self-consistently after startup. Figure 3 shows the time traces of the external heating waveforms, the central density, the contributions to the non-inductive current, the elongation, internal inductance and safety factor on-axis. Profiles of density, temperature and current and the free-boundary equilibrium at 3.5 s are also shown. Up to 4 MW of HHFW are used after startup from 50 ms and they are turned-off at 0.6 s, 100 ms after the NBI is turned-on. Turning-off the HHFW when the beams are turned-on is done for two reasons: (1) most of the power is absorbed on the fast ions and (2) the electron absorption of the HHFW drops reducing the fast wave driven current.

Density profiles are prescribed as a function of time, with the shape similar to the reference experiment and the whole profile rescaled to satisfy a constant fraction of the Greenwald density during H-mode. The rotation profile is taken from the experiment and is not rescaled to expected values on NSTX-U for the increased magnetic field and higher tangency radius, nor are the pedestal width and height. Considering the lower collisionality expected in NSTX-U, the density profiles assumed in H-mode in these simulations are probably too flat. Experiments on NSTX-U and systematic validation of transport will help refining these assumptions and improve the projections.

There is no feedback control on the density amplitude, but the input profiles are constructed to satisfy a constant Greenwald fraction, under the assumption that a non-inductive current ramp-up would require a minimum of 2.5 s to attain a target of 0.9 MA. This assumption is satisfied on average in the simulations, as it results from a number of runs that scan the ramp-up duration in inductive discharges and aim at minimizing the ohmic contribution for a fix beam configuration and an injected power of 10 MW. The simulation shown in Fig.3 assumes density of 75% of the Greenwald fraction. The L-H transition is set at 150 ms in the density rise and the profiles in H-mode are assumed to be flat, as shown in panel (e). Future simulations will use feedback control over the electron density amplitude [34] to ensure tracking of a particular Greenwald fraction throughout the plasma current ramp up.

Electron and ion temperature profiles are predicted during the RF phase with the

MMM7.1 transport model, which is found to reproduce amplitude and peaking of the experimental electron temperature profile in RF heated discharges, as well as both electron and ion temperature profiles in the NBI heated discharges at low current, as discussed in Sec.3. During the NBI phase and at current above 400 kA, the electron temperature is input as analytic form, while the ion temperature is predicted by the MMM7.1. In practice, the simulation is first run with predictive electron transport, then profiles after 0.5 s are replaced with analytic, broad profiles, rescaled to the central value predicted by the MMM7.1 model and the simulation is run a second time. Figure 3-(f) shows the profiles at 3.5 s. Ion and temperature profiles have comparable values on-axis and the ion temperature profile is more peaked than the electron temperature profile. These profiles are qualitatively consistent with the flattop measurements in the reference discharge.

Starting from the magnetic equilibrium of the reference discharge, we have first used `Isolver` standalone to reconstruct a sequence of boundary shapes in NSTX-U geometry consistent with the new poloidal field coil setup. This sequence of boundary shapes is then used by `Isolver` in TRANSP to converge the equilibrium solution to the desired shape with a χ^2 minimization. TRANSP will converge to a solution that satisfies the required shape and calculates the coil currents that are needed to converge to that solution. The χ^2 minimization is the first step required in the predictive calculations. When `Isolver` is run in χ^2 mode the coil currents are calculated at each time slice, which may cause discontinuities in the calculated currents. In a second step, the calculated currents are used as a reference and the simulation is run again with coil currents and plasma equilibrium evolved self-consistently as a circuit, with additional constraints to limit coil current excursions and with feedback control for the plasma horizontal and vertical position.

The initial value of current, when the simulation is started, is 300 kA, which is both consistent with inductive startup in NSTX, where the current is ramped fast to 300 kA in 50 ms, and with projections of up to 400 kA in CHI initiated plasmas on NSTX-U. In the simulation the Ohmic system cannot be excluded completely and the transition from inductive to non-inductive at 50 ms is imitated by a switch in the boundary conditions of the poloidal field diffusion equation solution, from matching the total current value to matching zero loop voltage. Like any inductive circuit, the plasma will respond to external forcing to avoid changes in the enclosed flux. In this case this is a current in the direction opposite to the non-inductive current, which will reduce the amplitude of the total current. In Fig.3-(d) this is seen as a drop in the ohmic contribution, which coincides with the increase in the direct fast wave driven current. Eventually the solution will converge to a steady state solution on the time scales of current diffusion, with zero ohmic current and 100% non-inductive current. This is indicated by the ohmic current decreasing in absolute value with progressing time.

The simulation scenario shown in Fig.3 achieves 700 kA of non-inductive current in about 2 s, and sustains confinement level of $H98 \simeq 1$, by using about 10 MW of Neutral Beam power. The current is sustained for the duration of the NBI pulse by a combination of

NBCD and bootstrap current, with comparable contributions.
The evolution of the internal inductance, of the elongation and of the safety value on-axis, shown in Fig.3-(d) reveal some of the typical problems encountered in simulations. First, the second beamline has high current-drive efficiency, which is good. However, the large beam pressure makes it difficult to maintain the plasma shape during the phase of non-inductive current sustainment. This is indicated in Fig.3-(e) by the slow decay of the elongation starting from 1.5 s and the slow increase in the internal inductance. This is the time when two sources at 80 kV are injected from the second beam line, with tangency radii of 110 and 120 cm. Injecting these sources any time before 1.5 s results in a lack of convergence in the equilibrium solution and in difficulties in sustaining the desired plasma shape. Injecting sources with lower energy would avoid this problem, but also sustain lower non-inductive current. The largest tangency radius line uses a source with 65 kV from 0.5 s, to help sustaining a broad current profile. Using higher energy sources exacerbate the issues with equilibrium convergence and plasma shape control mentioned above. The small tangency beam line is used from 0.5 s with all three sources at 80 kV.
Another issue encountered is maintaining the safety factor on-axis above one. It is found that operating with densities above 70% of the Greenwald limit, helps in maintaining $q > 1$ during the phase of sustainment of non-inductive current. The safety factor drops below unity also during the HHFW phase, mainly because of the large core current density. In the simulation in the figure, the rapid rise in the electron density helps maintaining values above unity, by reducing the fast wave current drive efficiency. These results indicate that a controlled evolution of the plasma density might be required for the control of the current profile and of the minimum safety factor.
These simulations assume no fast ion diffusion. Calculations in the flattop phase, under different assumptions on the diffusion coefficient, indicate a relaxation of the current profile and larger values of the minimum safety factor [6]. This will be addressed in future simulations, after characterization of the second beamline and experimental validation using TRANSP.
The outer gap in these simulations is about 12.5 cm and it is maintained fixed during the current ramp-up and sustainment phase, not an optimal value for ensuring broad deposition and optimal current profile control, as discussed by Gerhardt [6].
Figure 4 shows the variation in the non-inductive current when the density fraction is changed between 70% and 90% of the Greenwald limit, while maintaining fixed the NB configuration and the electron temperature profiles. Changing the density has a direct effect on the current drive efficiency and on the bootstrap current. However, the effects tend to compensate in the range of parameter considered, resulting in small variations of the non-inductive current. This suggests that the beam configuration (source energy and tangency radius) and how the beams are combined to ramp-up the current are the dominant factors that determine the achievement of a target operational space.
Figure 4(b) shows the simulation of an experiment on NSTX-U for optimization of the non-inductive current ramp-up, with magnetic field of 0.75 T. To demonstrate NBI

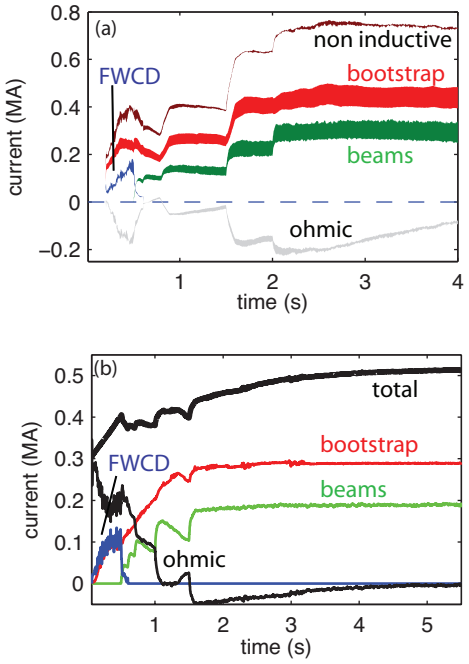

Figure 4. (a) Variation of current for densities between 70% and 90% of the Grenwald limit. (b) Simulation of an experiment for non-inductive ramp-up development at $B = 0.75$ T, where the discharge is ramped inductively for 0.5 s and then the OH coil is clamped.

sustainment, the current is ramped-up inductively and then the ohmic coils are clamped at 0.5 s. The current contribution in the figure shows that the discharge can be sustained non-inductively by the Neutral Beams starting from 1 s, and that the current can be ramped-up to 600 kA in about 5 s.

5. Addressing challenges to non-inductive ramp-up

Non-inductive ramp-up is challenging in both experiments and simulations, for several reasons. First, and obvious, one must provide sufficient current to replace the inductive current contribution. Contrary to an inductive discharge, where current diffuses from the outside, in a non-inductive ramp-up the externally driven current profiles are determined by the characteristics of the external sources. On NSTX-U, the HHFW would favor centrally peaked current and pressure profiles, while the NBI would provide more flexibility by combining sources with appropriate energy and tangency radii. In simulations, too peaked current profiles compromise the equilibrium convergence because of large gradients in space and time. Internal Transport Barriers develop in the presence of peaked pressure profiles during the HHFW phase, leading to simulations that are unstable against ballooning instabilities and that evolve into a disruption. A challenge is therefore finding a combination of heating and current drive sources that, in addition to satisfy the requirement of high current drive efficiency and accessibility

at low density and low temperature, also sustains MHD stable profiles.
This section shows that NBI are not effective at driving current on a low density, low temperature target, that HHFW can instead be used more effectively in the startup and that EC heating improves wave absorption and current drive efficiency of the HHFW. In the absence of a validated thermal transport model in these plasma regimes and of similar experiments on other devices to be used as a reference, the purpose of these simulations is not to provide solutions, but rather to address challenges and issues, as well as provide guidance for experimental validation. All simulations discussed in this section use a waveform for the plasma current, which has a fast ramp to 300 kA in 50 ms and then a slower ramp to 900 kA in 2.5 s. It is expected that CHI initiated discharges in NSTX-U will achieve currents up to 400 kA. The simulations use the total current as a boundary condition, thus the ohmic current profile will be determined by the difference between the target current and all the non-inductive contributions: bootstrap and externally driven current. The goal of the simulations is to maximize the non-inductive current after startup.

5.1. Using neutral beams at startup

In typical NSTX discharges beams are injected on the ohmic plasma at currents not less than 300 kA, to ensure confinement of the fast ions and maintain the shine-thru below 50% of the injected power, as well as to limit impurity accumulation. Figure 5 shows a simulation of the early ramp-up phase in NSTX-U geometry, with maximum nominal field of 1 T.
In this simulation the three sources at low-tangency radius are injected from 25 ms, and one source at higher tangency radius after 50 ms, in this sequence: 65 kV and 70 cm at 25 ms, 70 kV and 60 cm at 35 ms, 75 kV and 50 cm at 50 ms, 65 kV and 130 cm at 200 ms. Different combinations of sources in the first beam line result in variations in the driven current during the first 100 ms that are within 10% of the values shown. However, using higher energy sources and/or lower tangency radii in the second beam line results in large beam pressure and problems in the equilibrium calculations. In order to run more self-consistent simulations in this phase, the thermal transport, the beam heating and current and the fast-ion distribution have to be assessed. As seen in the figure, most of the power injected during the first 100 ms of discharge is lost via shine-thru, with orbit losses representing a constant contribution.
The level of current driven before 200 ms can probably be optimized with an adequate combination of the beam energy, tangency radius, and with a smart modulation, all options that will be addressed in dedicated experiments on NSTX-U. However, it appears from Fig.5 that the first 50 ms of discharge need an additional source of current that cannot be provided by the neutral beam injection only.

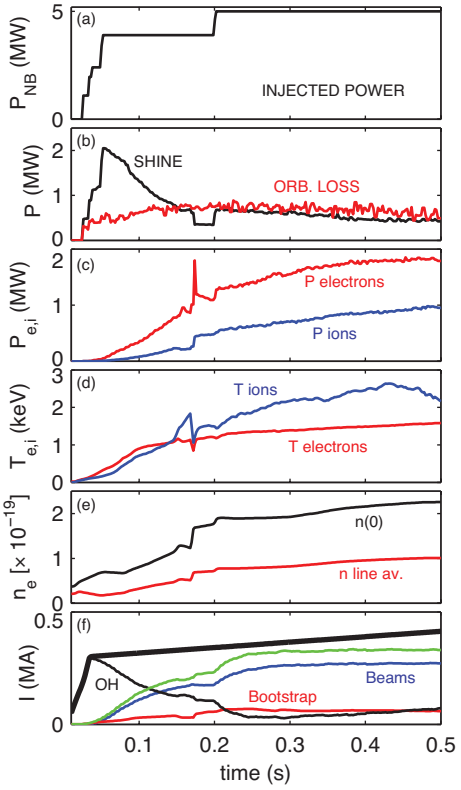

Figure 5. (a) NBI power waveform, (b) shine-thru and orbit loss power, (c) power absorbed on the electrons and on the ions, (d) central electron and ion temperature, (e) central and line averaged density, (f) plasma current waveform (black, thick) and contributions to the total current.

5.2. Driving current with HHFW at startup

Contrary to the Neutral Beams, the HHFW is effective at heating the plasma at low density, both in the electron and the ion channel, depending on the phasing of the antenna [20].

The hardware system allows power to be injected at a rate of 1 MW every ms. In practice, a significant fraction of the power can be lost to the scrape-off layer and deposited on the divertor, flowing to the magnetic field lines, rather than in the core plasma [19, 35]. The edge density value and the cut-off play an important role in the loss mechanisms [36]. These experimental conditions cannot be modeled with the tools available to us in time-dependent simulations. There is no model for the scrape-off-layer plasma in front of the antenna in TORIC, and all the input power is assumed to be absorbed. Losses are therefore taken into account by rescaling the input power to the simulation.

Figure 6 compares two cases that differ in the power step-up rate. In one case 4 MW are ramped-up in 100 ms, while in the second case they are ramped in 200 ms. These assumptions are equivalent to assuming that - for 6 MW injected with a square waveform - only a fraction is absorbed in the plasma, which gradually increases from a level of

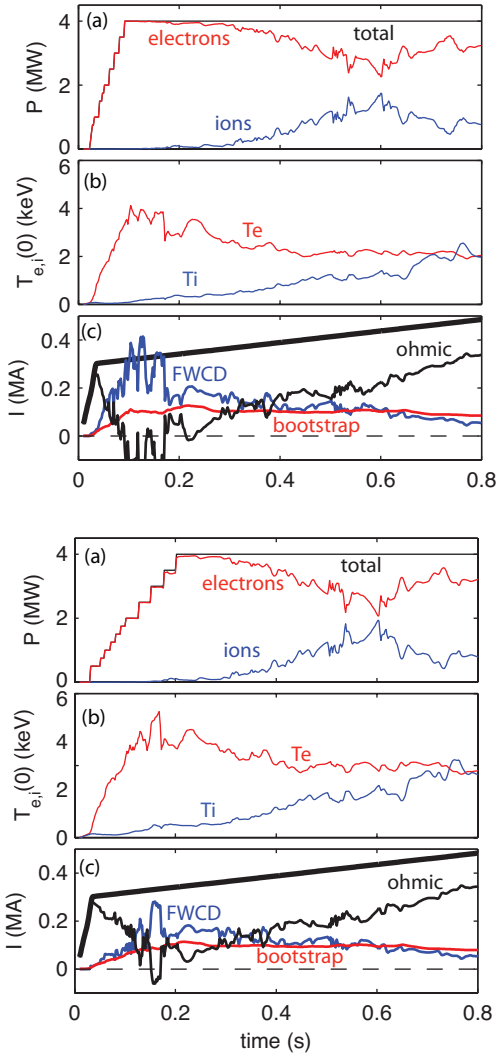

Figure 6. Comparison between two discharges with 4 MW of HHFW and different power ramp-up rate. (a) Injected power (black) and power absorbed on the electrons (red) and on the ions (blue). (b) central value of electron (red) and ion (blue) temperature. (c) total requested current (thick), bootstrap (red), FW (blue) ohmic (black) and non-inductive (green) current contribution.

about 10% to 65%. Stated differently, losses reduce from 90% at 20 ms down to 30% after 100 or 200 ms. Assuming that most of the power is lost at the earliest times is consistent with previous experiments on NSTX, where it proved to be difficult to couple the HHFW power in the CHI plasma target. On the other hand, assuming that the minimum level of losses is about 30% at 100 ms is probably optimistic at the light of those experiments. However, it is expected that at the higher magnetic field in NSTX-U and with the recent upgrade to the hardware, the scrape-off-layer losses will be significantly reduced. Figure 6 should therefore be interpreted as an indication of an upper limit to the fraction of allowable power loss in order to drive the current that is needed to ramp the current non-inductively.

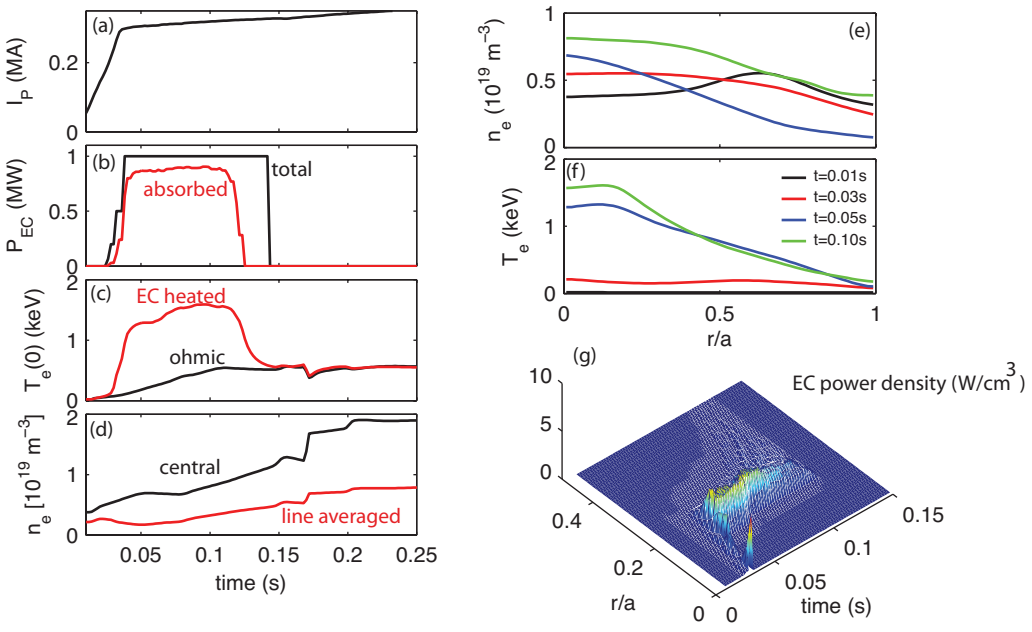

Figure 7. Left panel: time traces of (a) plasma current, (b) injected and absorbed power, (c) electron temperature on axis compared with an ohmic plasma, (d) central and line-averaged density. Right panel: profiles of (e) electron density (f) electron temperature and (g) EC heating profile.

The phasing of the antenna used here corresponds to a parallel wavenumber of 8 m^{-1}, the setting usually adopted in NSTX experiments. Simulations done using the three values of phasing indicate that this intermediate wavenumber is the most favorable for driving current in the startup plasma.

As shown in Fig.6, the driven current has a maximum in the first 200 ms of discharge, then it drops. The L-H transition is imposed in these simulations thru the density profile, which is analytic and prescribed in time, as shown in Fig.5-d. Increasing density decreases current drive efficiency, which is proportional to temperature and inversely proportional to density [37]. After 300 ms of discharge, the electron absorption also decreases, contributing to the drop in the calculated direct driven current.

Compared to the results shown in the previous section, it follows that - with these assumptions on the electron density evolution - the HHFW and the NBI do complement with each other, with the former being more effective at driving current after startup and the latter at subsequent times, when the efficiency of the HHFW decreases.

Providing good coupling of the HHFW to the low density, low temperature startup plasma is one of the challenges that need to be addressed in the first experimental campaign on NSTX-U.

6. Preparing a target plasma with ECH

Electron Cyclotron waves are a very effective mean for heating the NSTX-U startup plasma to high temperature in a short time, because of the good accessibility at low density. Figure 7 shows time-dependent simulations where the CHI target is heated with up to 1 MW of EC power. The target plasma (current, magnetic field) is the same used in the simulations discussed in the previous sections. Density and temperature profiles are taken from CHI experiments with solenoidal assist [11]. The initial electron temperature profile is evolved in time using the MMM7.1 transport model. Simulations with other transport models results in differences in the predicted temperature within 10% and are not shown here. The CHI target plasma has typically a very hollow temperature profile, which is peaked off-axis at about $r/a = 0.7$ and that has central values of about 10 eV. The density profile is also hollow at 10 ms and quickly broadens and flattens, with central value of about $0.5 \times 10^{19}\mathrm{m}^{-3}$. The evolution of the density and temperature profiles is shown in Fig.7-e,f respectively. The flattening in the temperature profile for $r/a < 0.2$ is a consequence of the highly localized heating profile, as shown in Fig.7-g.
In the simulations shown in Fig.7 the Electron Cyclotron heating is turned-on at 20 ms and the power stepped up to 1 MW within the first 35 ms of discharge. The absorption, initially very low, increases to 20% when the central temperature exceeds 400 eV and to 75% when the temperature exceeds 1 keV. For a more detailed analysis of first pass absorption for the O-mode injection in NSTX-U the reader is referred to the work by Taylor *et al* [23].
Figure 7-c shows a comparison with the simulation of an ohmic discharge, which uses the same density profiles, but no EC heating. Compared to the ohmic discharge, the EC waves are very effective at heating the plasma from a few tens of eV to about 1 keV in less than 30 ms. However, the plasma becomes overdense to the EC waves with increasing density, reducing the time window where the EC heating can be applied to the first 100-150 ms of discharge. The optimal density rise must be assessed in experiments and it will be a compromise between a desire for optimized EC heating and the need for avoiding impurity accumulation.

6.1. Improving HHFW access with ECH

Electron cyclotron waves heat the plasma very effectively to prepare a target where HHFW can be absorbed more favorably. Figure 8 compares two simulations with the same HHFW configuration, one with and one without EC. It is found that the fast wave direct current increases by about 10% when the HHFW is combined with the EC and it uses a phasing of $8\mathrm{m}^{-1}$. However, a significant improvement with respect to not using the EC occurs when the lowest phasing is used, as shown in Fig.8. Up to 3 MW of HHFW power are injected in the startup plasma, at a rate that corresponds to assuming between 60% and 75% losses during the EC heated phase. After the EC phase the HHFW power is stepped-up from 2 MW to 3 MW, equivalent to assuming that the losses reduce from 60% to 50%. The parallel wave vector used here, $k_{\|} = 3$

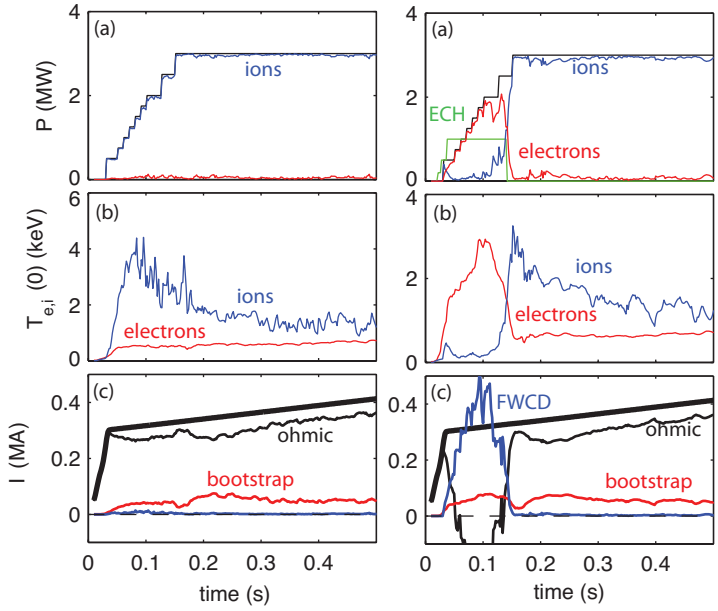

Figure 8. Comparison between two simulations without (left) and with EC heating (right) for parallel wavenumber of $k_{\|} = 3\mathrm{m}^{-1}$. (a) Injected power and power absorbed by the ions and the electrons. (b) central value of electron and ion temperature (c) total current waveform and contributions: ohmic (black), FWCD (blue), bootstrap (red).

m^{-1}, favors absorption on the thermal ions, as is shown in the left panel of Fig.8. In the case without EC the electron temperature remains in the range of 500 eV, there is almost no direct fast wave current and all the non-inductive current is driven by the bootstrap current.

When the plasma is pre-heated with 1 MW of EC, the electron temperature increases rapidly to the level of 1 keV, as discussed in the previous section. Although the antenna phasing is such to favor the ion absorption, a significant fraction of the power is predicted by TORIC to be absorbed on the electrons because of the large electron temperature. This corresponds also to a significant increase in the driven current during the EC phase. As little as 1-2 MW of absorbed HHFW power do suffice to drive 300 kA non-inductively, a significant improvement over using HHFW alone.

Ideally, a fully non-inductive startup and ramp-up should use all three sources to maximize benefits: the EC to pre-heat the CHI startup plasma and prepare a target plasma, the HHFW to maximize the non-inductive current at low density and then the NBI to ramp the current after the L-H transition, when the current drive efficiency of the HHFW is reduced. Figure 9 shows an example of non-inductive startup that uses all three sources. The HHFW should be used first with the lowest phasing, to take advantage of the synergy with the EC waves, then the phasing of the antenna can be increased to the maximum available, to reduce absorption on the fast ions and maximize the absorption on the electron. This would extend the HHFW phase, which might have

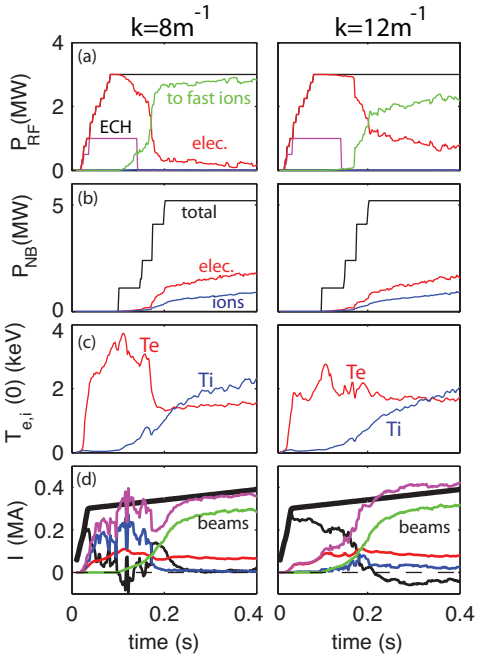

Figure 9. Simulations with EC, HHFW and NBI at startup for $k_{\|} = 8\mathrm{m}^{-1}$ (left) and for $k_{\|} = 13\mathrm{m}^{-1}$ (right). (a) EC waveform (magenta), HHFW injected power and power absorbed to the electrons (red), to the ions (blue) and to the fast ions (green). (b) Neutral Beam injected (black) power, and absorbed by the electrons (red) and by the ions (blue). (c) Central value of electron and ion temperature. (d) current waveform (thick black) and contributions: FWCD (blue), beam current (green), ohmic (black) and bootstrap (red), the total non-inductive current is also shown for comparison (magenta).

a positive impact on the control of impurity with central electron heating.

7. Conclusions

Non-solenoidal plasma formation and sustainment presents scientific and operational challenges, which are best addressed by fractioning the problem into its individual components.

First, there is the demonstration of non-inductive sustainment of plasmas that are MHD stable and that sustain adequate confinement level and optimal performance. This should be demonstrated at incrementally higher values of current. Second, the non-inductive sustainment needs to be extended back in time and to lower current, and possibly combined with control of the density evolution, beta and of the kinetic and current profiles. The phase right after startup is particularly challenging. The current decay following the CHI initiated plasma must be contrasted with externally driven contribution and this must be done by avoiding excessive core peaking of the current profiles. Radio-Frequency waves have good accessibility at low density and are effective at heating the low temperature startup plasma. However, a good absorption

of the HHFW must be ensured in startup conditions, as well as adequate control of the plasma position across the L-H transition, to avoid back transitions and RF power loss. Electron Cyclotron waves might be the only effective way of optimizing current drive at startup. By heating the plasma in the electron channel, the EC prepares a background plasma where HHFW can effectively drive current. By selecting an appropriate phasing of the antenna, the fast wave current drive efficiency is maximized and the constrains on the minimum required, absorbed power. With 1 MW of EC heating, as planned on the Upgrade, as little of 2 MW of HHFW would be needed to drive 300-400 kA.
Ideally, a fully non-inductive startup and ramp-up should use all three sources: the EC to pre-heat the CHI startup plasma, the HHFW to maximize non-inductive current at low density and NBI to ramp-up the current after the L-H transition, when the current drive efficiency of the HHFW is reduced. While the EC system would be available later, experiments at low current and low density to study the synergy between HHFW and NBI can be run already, in an attempt of minimizing power absorption to the fast ions, and maximizing current drive. Dynamical change of the antenna phasing might be an option to consider to broaden the current profiles at low current, when used in combination with Neutral Beams.
Independently of the combination of heating and current drive source, it is critical to demonstrate that the transient CHI can initiate a plasma with a current of at least 400 kA, in order to allow the other heating and current drive sources to take over and ramp-up the current non-inductively from there. Because of the scientific and operational challenges of plasma formation and sustainment without a central solenoid, the problem is best solved by dividing it into pieces and addressing issues individually while ensuring that the pieces are ultimately compatible and can be integrated. This approach applies to both experiments and simulations, in a loop where validation plays a critical role in the improvement of modeling and in the projection to new experiments.

Acknowledgements

S.M. Kaye and J. R. Wilson are acknowledged for carefully reading the manuscript. This work was supported by the U.S. Department of Energy under contract DE-AC02-CH0911466.

References

[1] Peng Y.-K.M. and Strickler D.J. (1986) Nucl.Fusion **26** 769
[2] PengY.-K.M., Galambos J.D. and Shipe P.C. (1992) Fusion Technol. **21** 1729
[3] Peng Y.-K.M. *et al* (2005) Plasma Phys. Control. Fusion **47** B263
[4] Peng Y.-K.M. *et al* (2009) Fusion Sci. Technol. **56** 957
[5] Menard J.E. *et al*, Nucl. Fusion **52** (2012) 083015
[6] Gerhardt S.P. *et al*, Nucl. Fusion **52** (2012) 083020
[7] Sabbagh S. *et al*, Nucl. Fusion (2006) **46** 635
[8] Jarboe T.R. Fusion Technol. (1989) **15** 7
[9] R. Raman *et al.*, Phys. Rev. Lett., **104**, 095003 (2010)

[10] Nelson B.A. *et al.*, Nucl. Fusion **51**, 063008 (2011)
[11] Raman R. *et al*, Nucl. Fusion **53** (2013) 073017
[12] R. Raman *et al.*, IEEE Transactions on Plasma Science, Vol **42**, 2154 (2014)
[13] Hawryluk R.J., An empirical approach to tokamak transport. In B. Coppi *et al*, editor, Physics close to thermonuclear conditions **1**, 19, Brussels, 1980. Commission of the European Communities.
[14] Andre R. TRANSP/PTRANSP Isolver Free Boundary Equilibrium Solver APS-DPP (2012) $http://w3.pppl.gov/\ randre/aps2012/APS2012_v3.pdf$
[15] Goldston R.J. *et al* (1981) J. Comput. Phys. **43** 61.
[16] Pankin A. *et al* (2004) Comput. Phys. Commun. **159** 157.
[17] Honda M., Kikuchi M., Azumi M., (2012) Nucl. Fusion **52** 023021
[18] Ono M. et al Nucl. Fusion (2000) **40** 557
[19] Hosea J., Bell R.E., LeBlanc B.P. *et al* Phys. Plasmas **15** (2008) 056104
[20] Bertelli N, *et al*, AIP Conf. Proc. **1580**, 310 (2014)
[21] Brambilla M. Plasma Phys. Controll. Fusion (2002) **44** 2423
[22] Taylor G., Ellis R.A., Harvey R.W., Hosea J.C and Smirnov A.P, EPJ Web of Conferences **32** (2012) 02014
[23] Taylor G., Ellis R.A., Fredd E., *et al*, EPJ Web of Conferences **xx** (2014) xxxx
[24] Harvey R.W. and McCoy M.G.. (1993) In Proceedings of the IAEA Technical Committee on Advances in Simulation and Modeling of Thermonuclear plasmas, 489, Vienna, IAEA.
[25] Smirnov A.P. *et al*, (2009) In Proceedings of the 15th Workshop on ECE and ECRH, 301. World scientific.
[26] Lin Liu Y.R., Chan V.S. and Prater R., (2008) Phys. Plasmas **6** 3934.
[27] Marushchenko et al, (2011) Phys. Plasmas **18** 032501.
[28] Taylor G. *et al*, Phys. Plasmas **19** (2012) 042501
[29] Gerhardt S.P. *et al*, Nucl. Fusion **51** (2011) 073031
[30] Rafiq T. *et al*, Phys. Plasmas **20** (2013) 032506
[31] Tang WM, Nucl. Fusion (1986) **26** 1605
[32] Honda M. and Fukuyama A., (2006) Nucl. Fusion **46** 580.
[33] Houlberg WA *et al*, Phys. Plasmas (1997) **4** 3230
[34] Boyer M. *et al*, Central safety factor and ?¡sub¿N¡/sub¿ control on NSTX-U via beam power and plasma boundary shape modification, using TRANSP for closed loop simulations accepted for publication, Nuclear Fusion.
[35] Perkins R.J. *et al*, Phys. Rev. Letters (2012) **109** 045001
[36] Bertelli et al, Nucl. Fusion **54** (2014) 083004.
[37] Fisch N.J, Rev. Mod. Phys. (1987) **59** 175

PPPL PRINCETON PLASMA PHYSICS LABORATORY

Princeton Plasma Physics Laboratory
Office of Reports and Publications

Managed by
Princeton University

under contract with the
U.S. Department of Energy
(DE-AC02-09CH11466)

P.O. Box 451, Princeton, NJ 08543
Phone: 609-243-2245
Fax: 609-243-2751

E-mail: publications@pppl.gov

Website: http://www.pppl.gov